

NEWTON-BASED OPTIMIZATION FOR NONNEGATIVE TENSOR FACTORIZATIONS

SAMANTHA HANSEN, TODD PLANTENGA, TAMARA G. KOLDA

Abstract. Tensor factorizations with nonnegative constraints have found application in analyzing data from cyber traffic, social networks, and other areas. We consider application data best described as being generated by a Poisson process (e.g., count data), which leads to sparse tensors that can be modeled by sparse factor matrices. In this paper we investigate efficient techniques for computing an appropriate tensor factorization and propose new subproblem solvers within the standard alternating block variable approach. Our new methods exploit structure and reformulate the optimization problem as small independent subproblems. We employ bound-constrained Newton and quasi-Newton methods. We compare our algorithms against other codes, demonstrating superior speed for high accuracy results and the ability to quickly find sparse solutions.

1. Introduction. Multilinear models have proved useful in analyzing data in a variety of fields. We focus on data that derives from a Poisson process, such as the number of packets sent from one IP address to another on a specific port [34], the number of papers published by an author at a given conference [15], or the count of emails between users in a given time period [4]. Data in these applications is nonnegative and often quite sparse, i.e., most tensor elements have a count of zero. The tensor factorization model corresponding to such sparse count data is computed from a nonlinear optimization problem that minimizes the Kullback-Leibler (K-L) divergence function and contains nonnegativity constraints on all variables.

In this paper we show how to make second-order optimization methods suitable for Poisson-based tensor models of large sparse count data. Multiplicative update is one of the most widely implemented methods for this model, but it suffers from slow convergence and inaccuracy in discovering the underlying sparsity. In large sparse tensors the application of nonlinear optimization techniques must consider sparsity and problem structure to get better performance. We show that by exploiting the partial separability of the subproblems we can successfully apply second order methods. We develop algorithms that scale to large sparse tensor applications, and are quick in identifying sparsity in the factors of the model.

There is a need for second order methods because we find that computing factor matrices to high accuracy, as measured by satisfaction of the first-order KKT conditions, is effective in revealing sparsity. By contrast, multiplicative update methods can make elements small but are slow at reaching the variable bound at zero, forcing the experimenter to guess when “small” means zero. We demonstrate that guessing a threshold is inherently difficult, making the high accuracy obtained with second order methods desirable.

We start from a standard Gauss-Seidel N -alternating block framework and show that each block subproblem is further separable into a set of independent functions, each of which depends on only a subset of variables. We optimize each subset of variables independently, an obvious idea which has nevertheless not previously appeared in the setting of sparse tensors. We call this a *row subproblem formulation* because the subset of variables corresponds to one row of a factor matrix. Each row subproblem amounts to minimizing a strictly convex function with nonnegativity constraints, which we solve using two-metric gradient projection techniques and exact or approximate second order information.

The importance of the row subproblem formulation is demonstrated in section 4.1, where we show that applying a second order methods directly to the block subproblem

is highly inefficient. We claim that a more effective way to apply second order methods is through the use of the row subproblem formulation.

Our contributions in this paper are as follows:

1. A new formulation for nonnegative tensor factorization based on the Kullback-Leibler divergence objective that allows for the effective use of second order optimization methods. The optimization problem is separated into row subproblems containing R variables, where R is the number of factors in the model. The formulation makes row subproblems independent, suggesting a parallel method, but we do not explore the potential in this paper.
2. Two Matlab algorithms for computing factorizations of sparse nonnegative tensors: one using second derivatives and the other using limited memory quasi-Newton approximations. The algorithms are made robust with an Armijo line search, damping modifications when the Hessian is ill-conditioned, and projections to the bound of zero based on two-metric gradient projection ideas in [7].
3. Test results that compare the performance of our two new algorithms with the best available multiplicative update method and a related quasi-Newton algorithm that does not formulate using row subproblems.
4. Test results showing the ability of our methods to quickly and accurately determine which elements of the factorization model are zero without using problem-specific thresholds.

The paper is outlined as follows: the remainder of Section 1 surveys related work and provides a review of basic tensor properties. Section 2 formalizes the Poisson nonnegative tensor factorization optimization problem, shows how the Gauss-Seidel alternating block framework can be applied, and converts the block subproblem into independent row subproblems. Section 3 outlines two algorithms for solving the row subproblem, one based on the damped Hessian (PDN-R for projected damped Newton), and one based on a limited memory approximation (PQN-R for projected quasi-Newton). Section 4 details numerical results on synthetic and real data sets and quantifies the accuracy of finding a truly sparse factorization. Section 5 contains a summary of the paper and concluding remarks.

1.1. Related Work. Nonnegative matrix factorization (NMF) is best known from the work of Lee and Seung [25, 26]. They considered both Gaussian and Poisson models, leading to least squares and K-L divergence objective functions, respectively. In both cases, they used an alternating variable block iterative method, i.e., a nonlinear block Gauss-Seidel method. Each block subproblem is convex, and a simple multiplicative update formula usually leads to an acceptable local minimum. Welling and Weber generalized NMF to the CANDECOMP/PARAFAC tensor factorization (NTF) [36].

In terms of the K-L version, it has been extended to a generalized K-L objective [14] as well as a Tucker tensor factorization [38]. Chi and Kolda provided an improved multiplicative update scheme for K-L that addressed performance and convergence issues as elements approach zero [10]; we compare to their method in Section 4. By interpreting the K-L divergence as an alternative Csiszar-Tusnday procedure, Zafeiriou and Petrou [39] provided a probabilistic interpretation of NTF along with a new multiplicative update scheme. The multiplicative update is equivalent to a scaled steepest descent step [26], so it is a first-order optimization method. Since our method uses second-order information, it allows for convergence to higher accuracy and a better determination of sparsity in the factorization.

Zdunek and Cichocki [40, 41] proposed a hybrid method for Blind Source Separation applications via NMF that used a damped Hessian method similar to ours. They recognized that the Hessian of the K-L objective has a block diagonal structure, but did not reformulate the optimization problem further as we do. Consequently, their Hessian matrix is large, and in both papers they switch to a least squares objective function for the larger mode of the matrix because their Newton method cannot scale up. Mixing objective functions in this manner is undesirable because it combines two different underlying models. As a point of comparison, a mode of size 1000 is considered too large for their Newton method [41], but our algorithm can factor a 200×1000 data set with $R = 10$ components to high accuracy in about ten minutes. The Hessian-based method in [41] has most of the advanced optimization features that we use (though details differ), including an Armijo line search, active set identification, and an adjustable Hessian damping factor.

Recently, Hsiel and Dhillon [19] report on an algorithm for NMF that updates one variable at a time, solving a nonlinear scalar function using Newton’s method with a constant step size. They achieve good performance for a least squares objective by taking the variables in a particular order based on gradient information; however, for the more complex K-L objective they must cycle through all the variables one by one. Our algorithms solve convex row subproblems with R variables using second order information; solving these subproblems one variable at a time by coordinate descent will likely have a much slower rate of convergence [30, pp 230-231].

A similar reformulation to ours was noted in earlier papers exploring the least squares function, but it was not used for Hessian-based methods or to exploit sparsity. Gonzales and Zhang used the reformulation with a multiplicative update method for NMF [17] but did not generalize to tensors or the K-L objective. Kim and Park used the reformulation for NTF [23], deriving small bound-constrained least squares subproblems. Their method solved the least squares subproblems by exact matrix factorization, without exploiting sparsity, and featured a block principal pivoting method for choosing the active set. Other works that solve the least squares norm objective by taking advantage of row by row or column by column subproblem decomposition include [11, 28].

Our algorithms are similar in spirit to the work of Kim et al. [20], which applied a projected quasi-Newton algorithm (called PQN in this paper) to solving NMF with a K-L objective. Like PQN, our algorithms identify active variables, compute a Newton-like direction in the space of free variables, and find a new iterate using a projected backtracking line search. We differ from PQN in reformulating the subproblem and in computing a damped Newton direction; both improvements make a huge difference in performance for large-scale tensor problems. We compare to PQN in Section 4.

There are many other works on the least squares version of NTF [8, 16, 21, 22, 23, 31, 32, 1, 27, 37]. In particular, all-at-once optimization methods, including Hessian-based algorithms, have been applied to nonnegative tensor factorization with a least squares objective function. Acar et al. considered conjugate gradient and nonlinear least squares methods on the full set of variables, though without nonnegativity constraints [1]. Paatero replaced the nonnegative constraints with a barrier function [31]. We are not aware of any work on all-at-once methods for the K-L objective in NTF.

Finally, we note that all methods, including ours, find only a locally optimal solution to the NTF problem. Vavasis proved that finding the global optimal solution in NMF is NP-hard [35].

1.2. Tensor Review. For a thorough introduction to tensors, see [24] and references therein; we only review concepts that are necessary for understanding this paper. A tensor is a multidimensional array. An N -way tensor \mathcal{X} has size $I_1 \times I_2 \times \dots \times I_N$. To differentiate between tensors, matrices, vectors, and scalars, we use the following notational convention: \mathcal{X} is a tensor (bold, capitalized, calligraphic), \mathbf{X} is a matrix (bold, capitalized), \mathbf{x} is a vector (bold, lower-case), and x is a scalar (lower-case). Additionally, given a matrix \mathbf{X} , \mathbf{x}_j denotes its j^{th} column and $\hat{\mathbf{x}}_i$ denotes its i^{th} row.

Just as a matrix can be decomposed into a sum of outer products between two vectors, an N -way tensor can be decomposed into a sum of outer products between N vectors. Each of these outer products (called components) yields an N -way tensor of rank one. The CP (CANDECOMP/PARAFAC) decomposition (or Kruskal form) [9, 18] represents a tensor as a sum of rank one tensors (see Figure 1.1):

$$\mathcal{X} = \left[\boldsymbol{\lambda}; \mathbf{A}^{(1)}, \dots, \mathbf{A}^{(N)} \right] = \sum_{r=1}^R \lambda_r \mathbf{a}_r^{(1)} \circ \dots \circ \mathbf{a}_r^{(N)} \quad (1.1)$$

where $\boldsymbol{\lambda}$ is a vector, and each $\mathbf{A}^{(n)}$ is an $I_n \times R$ factor matrix containing the R vectors contributed by mode n to the outer products; that is,

$$\mathbf{A}^{(n)} = [\mathbf{a}_1^{(n)} \dots \mathbf{a}_R^{(n)}]. \quad (1.2)$$

Equality holds in (1.1) when R equals the rank of \mathcal{X} , but often a tensor is approximated by a smaller number of terms. We let \mathbf{i} denote the multi-index (i_1, i_2, \dots, i_N) of an element $x_{\mathbf{i}}$ of \mathcal{X} .

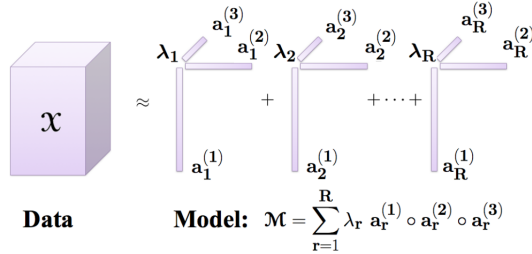


Fig. 1.1: CANDECOMP/PARAFAC decomposition of a 3-way tensor into R components.

We use the idea of matricization, or unfolding a tensor into a matrix. Specifically, unfolding along mode n yields a matrix of size $I_n \cdot J_n$, where

$$J_n = I_1 \cdot I_2 \cdot \dots \cdot I_{n-1} \cdot I_{n+1} \cdot \dots \cdot I_N.$$

We use the notation $\mathbf{X}_{(n)}$ to represent a tensor \mathcal{X} that has been unfolded into its n^{th} mode, and $x_{ij}^{(n)}$ for its (i, j) element. If a tensor \mathcal{X} is written in Kruskal form (1.1), then the n^{th} matricized mode is given by

$$\mathbf{X}_{(n)} = \mathbf{A}^{(n)} \boldsymbol{\Lambda} (\mathbf{A}^{(N)} \odot \dots \odot \mathbf{A}^{(n+1)} \odot \mathbf{A}^{(n-1)} \odot \dots \odot \mathbf{A}^{(1)})^T \quad (1.3)$$

where $\boldsymbol{\Lambda} = \text{diag}(\boldsymbol{\lambda})$ and \odot denotes the Khatri-Rao product [24].

Tensor factorization is the multidimensional analogue of matrix factorization and is an increasingly popular tool for analysis of multidimensional data sets. A CP tensor factorization seeks to model an N -way tensor \mathbf{X} as the sum of R rank one tensors as in equation (1.1). The case of $N = 2$ results in a matrix factorization model that can be expressed as $\mathbf{X} = \mathbf{A}^{(1)}\mathbf{\Lambda}(\mathbf{A}^{(2)})^T$.

Tensor results are generally easier to interpret when the factors (1.2) are sparse. Moreover, many sparse count applications can reasonably expect sparsity in the factors. For example, the 3-way data considered in [15] counts publications by authors at various conferences over a ten year period. The tensor representation has a sparsity of 0.14% (only 0.14% of the data elements are nonzero), and the factors computed by our algorithm with $R = 60$ (see section 4.2) have sparsity 9.3%, 2.7%, and 77.5% over the three modes. One meaning of sparsity in the factors is to say that a typical outer product term connects about 9% of the authors with 3% of the conferences in 8 of the 10 years. Linking particular authors and conferences is an important outcome of the tensor analysis, requiring clear distinction between zero and nonzero elements in the factors.

2. Poisson Nonnegative Tensor Factorization. In this section we state the optimization problem, examine its structure, and show how to separate it into simpler subproblems.

We seek a tensor model in CP form to approximate data \mathbf{X} :

$$\mathbf{X} \approx \mathcal{M} = \left[\boldsymbol{\lambda}; \mathbf{A}^{(1)}, \dots, \mathbf{A}^{(N)} \right] = \sum_{r=1}^R \lambda_r \mathbf{a}_r^{(1)} \circ \dots \circ \mathbf{a}_r^{(N)}.$$

The value of R is chosen empirically, and the scaling vector $\boldsymbol{\lambda}$ and factor matrices $\mathbf{A}^{(n)}$ are the model parameters that we compute.

In [10], it is shown that a K-L divergence objective function results when data elements follow Poisson distributions with multilinear parameters. The best-fitting tensor model under this assumption satisfies:

$$\begin{aligned} \min_{\boldsymbol{\lambda}, \mathbf{A}^{(1)}, \dots, \mathbf{A}^{(N)}} f(\mathcal{M}) &= \sum_{\mathbf{i}} m_{\mathbf{i}} - x_{\mathbf{i}} \log m_{\mathbf{i}} \\ \text{s.t. } \mathcal{M} &= \sum_{r=1}^R \lambda_r \mathbf{a}_r^{(1)} \circ \dots \circ \mathbf{a}_r^{(N)}, \end{aligned} \quad (2.1)$$

$$\lambda_r \geq 0, \mathbf{a}_r^{(n)} \geq 0, \|\mathbf{a}_r^{(n)}\|_1 = 1, \forall r \in \{1, \dots, R\}, \forall n \in \{1, \dots, N\}.$$

The model may have indices where $m_{\mathbf{i}} = 0$ and $x_{\mathbf{i}} = 0$; for this case we define $0 \log 0 = 0$. Note that for matrix factorization, (2.1) reduces to the K-L divergence proposed by Lee and Seung [25, 26]. The constraint that normalizes the column sum of the factor matrices serves to remove an inherent scaling ambiguity in the CP factor model.

As in [10], we unfold \mathbf{X} and \mathcal{M} into their n^{th} matricized mode, and use (1.3) to express the objective as

$$f(\mathcal{M}) = \mathbf{e}^T [\mathbf{A}^{(n)} \mathbf{\Lambda} \mathbf{\Pi}^{(n)} - \mathbf{X}_{(n)} * \log(\mathbf{A}^{(n)} \mathbf{\Lambda} \mathbf{\Pi}^{(n)})] \mathbf{e},$$

where \mathbf{e} is a vector of all ones, the operator $*$ denotes element-wise multiplication, $\log(\cdot)$ is taken element-wise, and

$$\begin{aligned}\mathbf{\Pi}^{(n)} &= (\mathbf{A}^{(N)} \odot \dots \odot \mathbf{A}^{(n+1)} \odot \mathbf{A}^{(n-1)} \odot \dots \odot \mathbf{A}^{(1)})^T \in \mathbf{R}^{R \times J_n}, \\ \mathbf{\Lambda} &= \text{diag}(\boldsymbol{\lambda}) \in \mathbf{R}^{R \times R}.\end{aligned}\quad (2.2)$$

Note that by expanding the Khatri-Rao products in (2.2) and remembering that column vectors $\mathbf{a}_r^{(n)}$ are normalized, each row of $\mathbf{\Pi}^{(n)}$ conveniently sums to 1. This is a consequence of using the ℓ_1 norm in (2.1).

The above representation of the objective motivates the use of an alternating block optimization method where only one factor matrix is optimized at a time. Holding the other factor matrices fixed, the optimization problem for $\mathbf{A}^{(n)}$ and $\mathbf{\Lambda}$ is

$$\begin{aligned}\min_{\mathbf{\Lambda}, \mathbf{A}^{(n)}} f(\mathbf{\Lambda}, \mathbf{A}^{(n)}) &= \mathbf{e}^T [\mathbf{A}^{(n)} \mathbf{\Lambda} \mathbf{\Pi}^{(n)} - \mathbf{X}_{(n)} * \log(\mathbf{A}^{(n)} \mathbf{\Lambda} \mathbf{\Pi}^{(n)})] \mathbf{e} \\ \text{s.t. } \mathbf{\Lambda} &\geq 0, \mathbf{A}^{(n)} \geq 0, \mathbf{e}^T \mathbf{A}^{(n)} = \mathbf{1}.\end{aligned}\quad (2.3)$$

Problem (2.3) is not convex. However, ignoring the equality constraint and letting $\mathbf{B}^{(n)} = \mathbf{A}^{(n)} \mathbf{\Lambda}$, we have

$$\min_{\mathbf{B}^{(n)} \geq 0} f(\mathbf{B}^{(n)}) = \mathbf{e}^T [\mathbf{B}^{(n)} \mathbf{\Pi}^{(n)} - \mathbf{X}_{(n)} * \log(\mathbf{B}^{(n)} \mathbf{\Pi}^{(n)})] \mathbf{e} \quad (2.4)$$

which is convex with respect to $\mathbf{B}^{(n)}$. The two formulations are equivalent in that a KKT point of (2.4) can be used to find a KKT point of (2.3). Chi and Kolda show in [10] that (2.4) is *strictly* convex given certain assumptions on the sparsity pattern of $\mathbf{X}_{(n)}$.

We pause to think about (2.4) when the tensor is 2-way. In this case we solve for two factor matrices by alternating over two block subproblems; for instance, with $n = 1$ the subproblem (2.4) finds $\mathbf{B}^{(1)}$ with $\mathbf{\Pi}^{(1)} = (\mathbf{A}^{(2)})^T$. For an N -way problem the only change to (2.4) is $\mathbf{\Pi}^{(n)}$, which grows in size exponentially with each additional factor matrix. To efficiently compute the subproblems (2.4) for large sparse tensors we need to avoid forming $\mathbf{\Pi}^{(n)}$ all at once, and this is exactly what our row subproblem formulation (section 2.1) accomplishes.

At this point we define Algorithm 1, a Gauss-Seidel alternating block method. The algorithm iterates over each mode of the tensor, solving a convex optimization subproblem. Steps 6 and 7 rescale the factor matrix columns, redistributing the weight into $\boldsymbol{\lambda}$. For the moment, we leave the subproblem solution method in step 5 unspecified. A proof that Algorithm 1 converges to a local minimum of (2.1) is given in [10].

This outline of Algorithm 1 corresponds exactly with the method proposed in [10]; where we differ is in how to solve subproblem (2.4) in step 5. Note also that this algorithm is the same as for the least squares objective (references were given in section 1.1); there the subproblem in step 5 is replaced by a linear least squares subproblem. We now proceed to describe our method for solving (2.4).

2.1. Row Subproblem Reformulation. We examine the objective function $f(\mathbf{B}^{(n)})$ in (2.4) and show that it can be reformulated into independent functions. As mentioned in the previous section, rows of $\mathbf{\Pi}^{(n)}$ sum to one if the columns of factor matrices are nonnegative and sum to one. When $\mathbf{\Pi}^{(n)}$ is formed at step 4 of

Algorithm 1 Alternating Block Framework

Given tensor sizes I_1, \dots, I_N , the number of components R , and data tensor \mathfrak{X}
Return a model $\mathcal{M} = [\boldsymbol{\lambda}; \mathbf{A}^{(1)} \dots \mathbf{A}^{(N)}]$

- 1: Initialize $\mathbf{A}^{(n)} \in \mathbf{R}^{I_n \times R}$ for $n = 1, \dots, N$
 - 2: **repeat**
 - 3: **for** $n = 1, \dots, N$ **do**
 - 4: Let $\boldsymbol{\Pi}^{(n)} = (\mathbf{A}^{(N)} \odot \dots \odot \mathbf{A}^{(n+1)} \odot \mathbf{A}^{(n-1)} \odot \dots \odot \mathbf{A}^{(1)})^T$
 - 5: Use Algorithm 2 to compute \mathbf{B}^* that minimizes $f(\mathbf{B}^{(n)})$ s.t. $\mathbf{B}^{(n)} \geq 0$
 - 6: $\boldsymbol{\lambda} \leftarrow \mathbf{e}^T \mathbf{B}^*$
 - 7: $\mathbf{A}^{(n)} \leftarrow \mathbf{B}^* \boldsymbol{\Lambda}^{-1}$, where $\boldsymbol{\Lambda} = \text{diag}(\boldsymbol{\lambda})$
 - 8: **end for**
 - 9: **until** all mode subproblems have converged
-

Algorithm 1, the factor matrices satisfy these conditions by virtue of steps 6 and 7; hence, the first term of $f(\mathbf{B}^{(n)})$ is

$$\mathbf{e}^T \mathbf{B}^{(n)} \boldsymbol{\Pi}^{(n)} \mathbf{e} = \mathbf{e}^T \mathbf{B}^{(n)} \mathbf{e} = \sum_{i=1}^{I_n} \sum_{r=1}^R b_{ir}^{(n)}.$$

The second term of $f(\mathbf{B}^{(n)})$ is a sum of elements from the $I_n \times J_n$ matrix $\mathbf{X}_{(n)} * \log(\mathbf{B}^{(n)} \boldsymbol{\Pi}^{(n)})$. Recall that the operations in this expression are element-wise, so the scalar matrix element (i, j) of the term can be written as

$$x_{ij}^{(n)} \log \left(\sum_{r=1}^R b_{ir}^{(n)} \pi_{rj}^{(n)} \right).$$

Adding all the elements and combining with the first term gives

$$\begin{aligned} f(\mathbf{B}^{(n)}) &= \sum_{i=1}^{I_n} \sum_{r=1}^R b_{ir}^{(n)} - \sum_{i=1}^{I_n} \sum_{j=1}^{J_n} x_{ij}^{(n)} \log \left(\sum_{r=1}^R b_{ir}^{(n)} \pi_{rj}^{(n)} \right) \\ &= \sum_{i=1}^{I_n} f_{\text{row}}(\hat{\mathbf{b}}_i^{(n)}, \hat{\mathbf{x}}_i^{(n)}, \boldsymbol{\Pi}^{(n)}). \end{aligned}$$

where $\hat{\mathbf{b}}_i$ and $\hat{\mathbf{x}}_i$ are the i^{th} row vectors of their corresponding matrices, and

$$f_{\text{row}}(\hat{\mathbf{b}}, \hat{\mathbf{x}}, \boldsymbol{\Pi}) = \sum_{r=1}^R \hat{b}_r - \sum_{j=1}^{J_n} \hat{x}_j \log \left(\sum_{r=1}^R \hat{b}_r \pi_{rj} \right). \quad (2.5)$$

Problem (2.4) can now be rewritten as

$$\min_{\hat{\mathbf{b}}_1, \dots, \hat{\mathbf{b}}_{I_n} \geq 0} \sum_{i=1}^{I_n} f_{\text{row}}(\hat{\mathbf{b}}_i^{(n)}, \hat{\mathbf{x}}_i^{(n)}, \boldsymbol{\Pi}^{(n)}). \quad (2.6)$$

This is a completely separable set of I_n row subproblems, each one a convex non-linear optimization problem containing R variables. The relatively small number of

Algorithm 2 Row Subproblem Framework for Solving (2.6)

Given $\mathbf{X}_{(n)}$ of size $I_n \times J_n$, and $\mathbf{\Pi}^{(n)}$ of size $R \times J_n$

Return a solution \mathbf{B}^* consisting of row vectors $\hat{\mathbf{b}}_1^*, \dots, \hat{\mathbf{b}}_{I_n}^*$

- 1: **for** $i = 1, \dots, I_n$ **do**
- 2: Select row $\hat{\mathbf{x}}_i$ of $\mathbf{X}_{(n)}$
- 3: Generate one column of $\mathbf{\Pi}^{(n)}$ for each nonzero in $\hat{\mathbf{x}}_i$
- 4: Use Algorithm 3 or 4 to compute $\hat{\mathbf{b}}_i^*$ that solves

$$\min f_{\text{row}}(\hat{\mathbf{b}}_i^{(n)}, \hat{\mathbf{x}}_i^{(n)}, \mathbf{\Pi}^{(n)}) \text{ subject to } \hat{\mathbf{b}}_i \geq 0$$

- 5: **end for**
-

variables makes second-order optimization methods tractable, and that is the direction we pursue in this paper. Algorithm 2 describes how the reformulation fits into Algorithm 1.

The independence of row subproblems is crucial for handling large tensors. For example, if a 3-way tensor of size $1000 \times 1000 \times 1000$ is factored into $R = 100$ components, then $\mathbf{\Pi}^{(n)}$ is a 100×10^6 matrix. However, elements of $\mathbf{\Pi}^{(n)}$ appear in the optimization objective only where the matricized tensor $\mathbf{X}_{(n)}$ has nonzero elements, so in a sparse tensor many columns of $\mathbf{\Pi}^{(n)}$ can be ignored; this point was first published in [10]. Algorithm 2 exploits this fact in step 3. Observe that step 4 of Algorithm 1 computes columns of $\mathbf{\Pi}^{(n)}$ for nonzero elements in all of $\mathbf{X}_{(n)}$, while the row subproblem does so for only nonzero elements in row $\hat{\mathbf{x}}_i$.

Algorithm 2 also points the way to a parallel implementation of the CP tensor factorization. We note that each row subproblem can be run in parallel, and storage costs are determined by the sparsity of the data. In a distributed computing architecture an algorithm could identify the nonzero elements of each row subproblem at the beginning of execution and collect only the data needed to form appropriate columns of $\mathbf{\Pi}^{(n)}$ at a given processing element. We do not implement a parallel version of the algorithm in this paper.

3. Solving the Row Subproblem. In this section we show how to solve the row subproblem (2.6) using second-order information. We describe two algorithms, one applying second derivatives in the form of a damped Hessian matrix, and the other using a quasi-Newton approximation of the Hessian. Both algorithms use projection, but the details differ.

Each row subproblem consists of minimizing a strictly convex function of R variables with nonnegativity constraints. One of the most effective methods for solving bound constrained problems is second-order gradient projection; cf. [33]. We employ a form of two-metric gradient projection from Bertsekas [7]. Each variable is marked in one of three states based on its gradient and current location: fixed at its bound of zero, allowed to move in the direction of steepest descent, or free to move along a Newton or quasi-Newton search direction; details are in section 3.1.

An alternative to Bertsekas is to use methods that employ gradient projection searches to determine the active variables (those set to zero). Examples include the generalized Cauchy point [12] and gradient projection along the steepest descent direction with a line search. We experimented with using the generalized Cauchy point to determine the active variables, but preliminary results indicated that this approach sets too many variables to be at their bound, leading to more iterations and poor

overall performance. Gradient projection steps with a line search calls for an extra function evaluation, which is computationally expensive. Given a more efficient method for evaluating the function, this might be a better approach since, under mild conditions, gradient projection methods find the active set in a finite number of iterations [6].

For notational convenience, in this section we use \mathbf{b} for the column vector representation of row vector $\hat{\mathbf{b}}_i$; that is, $\mathbf{b} = \hat{\mathbf{b}}_i^T$. Iterations are denoted with superscript k , and ∇_r represents the derivative with respect to the r^{th} variable. Let $P_+[\mathbf{v}]$ be the projection operator that restricts each element of vector \mathbf{v} to be nonnegative. We make use of the first and second derivatives of f_{row} , given by

$$\begin{aligned}\nabla_r f_{\text{row}}(\mathbf{b}) &= \frac{\partial f_{\text{row}}(\mathbf{b}, \mathbf{x}, \mathbf{\Pi})}{\partial b_r} = 1 - \sum_{j=1}^{J_n} \frac{x_j \pi_{rj}}{\sum_{i=1}^R b_i \pi_{ij}}, \\ \nabla_{rs}^2 f_{\text{row}}(\mathbf{b}) &= \frac{\partial^2 f_{\text{row}}(\mathbf{b}, \mathbf{x}, \mathbf{\Pi})}{\partial b_r \partial b_s} = \sum_{j=1}^{J_n} \frac{x_j \pi_{rj} \pi_{sj}}{(\sum_{i=1}^R b_i \pi_{ij})^2}.\end{aligned}\quad (3.1)$$

3.1. Two-Metric Projection. At each iteration k we must choose a set variables to update such that progress is made in decreasing the objective. Bertsekas demonstrated in [7] that iterative updates of the form

$$\mathbf{b}^{k+1} = P_+[\mathbf{b}^k - \alpha \mathbf{M}^k \nabla f_{\text{row}}(\mathbf{b}^k)]$$

are not guaranteed to decrease the objective function unless \mathbf{M}^k is a positive diagonal matrix. Instead, it is necessary to predict the variables that have the potential to make progress in decreasing the objective, and then update just those variables using a positive definite matrix. We present the two-metric technique of Bertsekas as it is executed in our algorithm, which differs superficially from the presentation in [7].

A variable's potential effect on the objective is determined by how close it is to zero and by its direction of steepest descent. If a variable is close to zero and its steepest descent direction points towards the negative orthant, then the next update will most likely project the variable to zero and its small displacement will have little effect on the objective. A closeness threshold ϵ_k is computed from a user defined parameter $\epsilon > 0$ as

$$\epsilon_k = \min(w_k, \epsilon), \quad w_k = \left\| \mathbf{b}^k - P_+[\mathbf{b}^k - \nabla f_{\text{row}}(\mathbf{b}^k)] \right\|_2. \quad (3.2)$$

We then define index sets

$$\begin{aligned}\mathcal{A}(\mathbf{b}^k) &= \left\{ r \mid b_r^k = 0, \nabla_r f_{\text{row}}(\mathbf{b}^k) > 0 \right\}, \\ \mathcal{G}(\mathbf{b}^k) &= \left\{ r \mid 0 < b_r^k \leq \epsilon_k, \nabla_r f_{\text{row}}(\mathbf{b}^k) > 0 \right\}, \\ \mathcal{F}(\mathbf{b}^k) &= \left(\mathcal{A}(\mathbf{b}^k) \cup \mathcal{G}(\mathbf{b}^k) \right)^c.\end{aligned}\quad (3.3)$$

Variables in the set \mathcal{A} are fixed at zero, variables in \mathcal{G} move in the direction of the negative gradient, and variables in \mathcal{F} are free to move according to second-order information. Note that if $\epsilon = 0$ then $\epsilon_k = 0$, \mathcal{G} is empty, and the method reduces to defining an active set of variables by instantaneous line search [3]; we use this in the quasi-Newton method described in section 3.2.

3.1.1. Damped Newton Step. The damped Newton direction is taken with respect to only the variables in the set \mathcal{F} from (3.3). Let

$$\mathbf{g}_F^k = [\nabla f_{\text{row}}(\mathbf{b}^k)]_{\mathcal{F}}, \quad \mathbf{H}_F^k = [\nabla^2 f_{\text{row}}(\mathbf{b}^k)]_{\mathcal{F}}, \quad \mathbf{b}_F^k = [\mathbf{b}^k]_{\mathcal{F}},$$

where $[\mathbf{v}]_{\mathcal{F}}$ chooses the elements of vector \mathbf{v} corresponding to variables in the set \mathcal{F} . Since the row subproblems are strictly convex, the full Hessian and \mathbf{H}_F^k are positive definite.

The damped Hessian has its roots in trust region methods. At every iteration we form a quadratic approximation m_k of the objective plus a quadratic penalty. The penalty serves to ensure that the next iterate does not move too far away from the current iterate, which is important when the Hessian is ill-conditioned. The quadratic model plus penalty expanded about \mathbf{b}^k for variables $\mathbf{d}_F \in \mathbb{R}^{|\mathcal{F}|}$ is

$$m_k(\mathbf{d}_F; \mu_k) = f_{\text{row}}(\mathbf{b}^k) + \mathbf{d}_F^T \mathbf{g}_F^k + \frac{1}{2} \mathbf{d}_F^T \mathbf{H}_F^k \mathbf{d}_F + \frac{\mu_k}{2} \|\mathbf{d}_F\|_2^2. \quad (3.4)$$

The unique minimum of $m_k(\cdot)$ is

$$\mathbf{d}_F^k = -(\mathbf{H}_F^k + \mu_k \mathbf{I})^{-1} \mathbf{g}_F^k,$$

where $\mathbf{H}_F^k + \mu_k \mathbf{I}$ is known as the damped Hessian. Adding a multiple of the identity to \mathbf{H}_F^k increases each of its eigenvalues by μ_k , which has the effect of diminishing the length of \mathbf{d}_F^k , similar to the action of a trust region. The step \mathbf{d}_F^k is computed using a Cholesky factorization of the damped Hessian, and the full space search direction $\mathbf{d}^k \in \mathbb{R}^R$ is then given by

$$d_r^k = \begin{cases} (\mathbf{d}_F^k)_r & r \in \mathcal{F} \\ -\nabla_r f_{\text{row}}(\mathbf{b}^k) & r \in \mathcal{G} \\ 0 & r \in \mathcal{A}, \end{cases} \quad (3.5)$$

where index sets \mathcal{A} , \mathcal{G} , and \mathcal{F} are defined in (3.3).

The damping parameter μ_k is adjusted by a Levenberg-Marquardt strategy [30]. First define the ratio of actual reduction over predicted reduction,

$$\rho = \frac{f_{\text{row}}(\mathbf{b}^k + \mathbf{d}^k) - f_{\text{row}}(\mathbf{b}^k)}{m_k(\mathbf{d}_F^k; 0) - m_k(0; 0)}, \quad (3.6)$$

where $m_k(\cdot)$ is defined by (3.4). Note the numerator of (3.6) calculates f_{row} using all variables, while the denominator calculates $m_k(\cdot)$ using only the variable in \mathcal{F} . The damping parameter is updated by the following rule

$$\mu_{k+1} = \begin{cases} \frac{7}{2} \mu_k & \text{if } \rho < \frac{1}{4} \\ \frac{2}{7} \mu_k & \text{if } \rho > \frac{3}{4} \\ \mu_k & \text{otherwise.} \end{cases} \quad (3.7)$$

Since \mathbf{d}_F^k is the minimum of (3.4), the denominator of (3.6) is always negative. If the search direction \mathbf{d}^k increases the objective function, then the numerator of (3.6) will be positive; hence $\rho < 0$ and the damping parameter will be increased for the next iteration. On the other hand, if the search direction \mathbf{d}^k decreases the objective function, then the numerator will be negative; hence $\rho > 0$ and the relative sizes of the actual reduction and predicted reduction will determine how the damping parameter is adjusted.

3.1.2. Line Search. After computing the search direction \mathbf{d}^k , we ensure the next iterate decreases the objective by using a projected back-tracking line search that satisfies the Armijo condition [30]. Given scalars $0 < \beta$ and $\sigma < 1$, we find the smallest integer t that satisfies the inequality

$$f_{\text{row}}(P_+[\mathbf{b}^k + \beta^t \mathbf{d}^k]) - f_{\text{row}}(\mathbf{b}^k) \leq \sigma(P_+[\mathbf{b}^k + \beta^t \mathbf{d}^k] - \mathbf{b}^k)^T \nabla f_{\text{row}}(\mathbf{b}^k). \quad (3.8)$$

We set $\alpha_k = \beta^t$ and the next iterate is given by

$$\mathbf{b}^{k+1} = P_+[\mathbf{b}^k + \alpha_k \mathbf{d}^k].$$

3.2. Projected Quasi-Newton Step. As an alternative to the damped Hessian step, we adapt the projected quasi-Newton step from [20]. Their work employs a limited memory BFGS (L-BFGS) approximation [29] in a framework suitable for any convex, bound constrained problem.

L-BFGS estimates Hessian properties based on the most recent M update pairs $\{\mathbf{s}^i, \mathbf{y}^i\}$, $i \in [\max\{1, k - M\}, k]$, where

$$\mathbf{s}^k = \mathbf{b}^{k+1} - \mathbf{b}^k, \quad \mathbf{y}^k = \nabla f_{\text{row}}(\mathbf{b}^{k+1}) - \nabla f_{\text{row}}(\mathbf{b}^k). \quad (3.9)$$

L-BFGS uses a two-loop recursion through the stored pairs to efficiently compute a vector $\mathbf{p}^k = \bar{\mathbf{H}}^k \mathbf{g}^k$, where $\bar{\mathbf{H}}^k$ approximates the inverse of the Hessian \mathbf{H}^k using the pairs $\{\mathbf{s}^i, \mathbf{y}^i\}$. Storage is set to $M = 3$ pairs in all experiments. See Chapter 7 of [30] for further detail.

The projected quasi-Newton search direction \mathbf{d}^k , analogous to (3.5), is

$$d_r^k = \begin{cases} -p_r^k & r \in \mathcal{F} \\ 0 & r \in \mathcal{A}, \end{cases} \quad (3.10)$$

where \mathcal{F} and \mathcal{A} are determined from (3.3) with $\epsilon = 0$ in (3.2). Although $\epsilon = 0$ forfeits the guarantee of convergence in solving the row subproblem (see section 3.1), we argue that it improves the accuracy of the computed step \mathbf{d}^k in (3.10).

The inverse Hessian approximation $\bar{\mathbf{H}}^k$ is built from update pairs that span the full space of variables. This is necessary because the subspace of free variables can change at every iteration. Ideally, (3.10) should compute the step for variables in \mathcal{F} using only second-order information pertaining to those variables, as is done with $\mathbf{d}_{\mathcal{F}}^k$ in (3.5). Instead, \mathbf{p}^k is computed over all variables and then (3.10) zeroes out the step for variables not in \mathcal{F} .

We can express this difference in terms of the reduced Hessian. Let \mathbf{B} denote the true Hessian matrix. Suppose the variables in \mathcal{F} are the first $1, \dots, |\mathcal{F}|$ variables, and the remaining variables are in $\mathcal{N} = \mathcal{A} \cup \mathcal{G}$. Write \mathbf{B} in block form as

$$\mathbf{B} = \begin{bmatrix} \mathbf{B}_{FF} & \mathbf{B}_{NF}^T \\ \mathbf{B}_{NF} & \mathbf{B}_{NN} \end{bmatrix},$$

with $\mathbf{B}_{FF} \in \mathbb{R}^{|\mathcal{F}| \times |\mathcal{F}|}$, $\mathbf{B}_{NF} \in \mathbb{R}^{|\mathcal{N}| \times |\mathcal{F}|}$, and $\mathbf{B}_{NN} \in \mathbb{R}^{|\mathcal{N}| \times |\mathcal{N}|}$. In (3.5) we use the reduced inverse Hessian; that is, $\mathbf{H}_F = \mathbf{B}_{FF}^{-1}$. To get (3.10) we form the inverse of the Hessian over all variables and take just the rows and columns corresponding to variables in \mathcal{F} , expressed as $[\mathbf{B}^{-1}]_{\mathcal{F}}$. Assuming the Schur complement exists,

$$[\mathbf{B}^{-1}]_{\mathcal{F}} = (\mathbf{B}_{FF} - \mathbf{B}_{NF}^T \mathbf{B}_{NN}^{-1} \mathbf{B}_{NF})^{-1},$$

and we see that this differs from \mathbf{H}_F by the term $\mathbf{B}_{NF}^T \mathbf{B}_{NN}^{-1} \mathbf{B}_{NF}$, a matrix of rank $|\mathcal{N}|$. Hence, if $|\mathcal{N}|$ is small then the difference should be less, which is precisely the effect we get by using $\epsilon = 0$ in (3.2).

3.3. Stopping Criterion. Since the row subproblems are convex, any point satisfying the first-order KKT conditions is an optimal solution. Specifically, \mathbf{b}^* is a KKT point of (2.6) if it satisfies

$$\nabla f_{\text{row}}(\mathbf{b}^*) - \mathbf{v}^* = \mathbf{0}, \quad (\mathbf{b}^*)^T \mathbf{v}^* = 0, \quad \mathbf{b}^* \geq \mathbf{0}, \quad \mathbf{v}^* \geq \mathbf{0},$$

where \mathbf{v}^* is the vector of dual variables associated with the nonnegativity constraints. Knowing the algorithm keeps all iterates \mathbf{b}^k nonnegative, we can express the KKT condition for component r as

$$\left| \min\{b_r^k, \nabla_r f_{\text{row}}(\mathbf{b}^k)\} \right| = 0.$$

A suitable stopping criterion is to approximately satisfy the KKT conditions to a tolerance $\tau > 0$. We achieve this by requiring that all row subproblems satisfy

$$\text{kkt}_{\text{viol}} = \max_r \left\{ \left| \min\{b_r^k, \nabla_r f_{\text{row}}(\mathbf{b}^k)\} \right| \right\}. \quad (3.11)$$

The full algorithm solves to an overall tolerance τ when the kkt_{viol} of every row subproblem satisfies (3.11). This condition is enforced for all the row subproblems (step 4 of Algorithm 2) generated from all the tensor modes (step 5 of Algorithm 1). Note that enforcement requires examination of kkt_{viol} for all row subproblems whenever the solution of any subproblem mode is updated, because the solution modifies the $\mathbf{\Pi}^{(n)}$ matrices of other modes.

3.4. Row Subproblem Algorithms. Having described the ingredients, we pull everything together into complete algorithms for solving the row subproblem in step 4 of Algorithm 2. We present two methods in Algorithm 3 and Algorithm 4: PDN-R uses a damped Hessian matrix within a two-metric projection framework, and PQN-R uses a quasi-Newton Hessian approximation with instantaneous line search (the ‘-R’ designates a row subproblem formulation).

As mentioned, PQN-R is related to [20]. Specifically, we note

1. The free variables chosen in step 7 of PQN-R are found with $\epsilon = 0$ in (3.2), the same as in [20]; however, PDN-R uses $\epsilon = 10^{-3}$.
2. The line search in step 9 of PQN-R and step 11 of PDN-R satisfies the Armijo condition. This differs from [20], which used $\sigma \alpha (\mathbf{d}^k)^T \nabla f_{\text{row}}(\mathbf{b}^k)$ on the right-hand side of (3.8). We use (3.8) because it correctly measures predicted progress. In particular, it is easier to satisfy when $(\mathbf{d}^k)^T \nabla f_{\text{row}}(\mathbf{b}^k)$ is large and many variables hit their bound for small α .
3. Updates to the L-BFGS approximation in step 11 of PQN-R are unchanged from [20]. Information is included from all row subproblem variables, whether active or free.

4. Experiments. This section characterizes the performance of our algorithms, comparing them with multiplicative update [10] and second order methods that do not use the row subproblem formulation. All algorithms fit in the alternating block framework of Algorithm 1, differing in how they solve (2.4).

Our two algorithms are the projected damped Hessian method (PDN-R), and the projected quasi-Newton method (PQN-R), from the pseudo-code of Algorithms 3 and 4; recall that ‘-R’ means the row subproblem formulation is applied. In this paper we do not tune the algorithms to each test case, but instead chose a single set of parameter values: $\mu_0 = 10^{-5}$, $\sigma = 10^{-4}$, and $\beta = 1/4$. The bound constraint

Algorithm 3 Projected Newton-Based Solver PDN-R for the Row Subproblem

Given data $\hat{\mathbf{x}}$ and $\mathbf{\Pi}$, constants $\mu_0, \sigma, \beta, K_{\max}$, stop tolerance τ , and initial values \mathbf{b}^0
 Return a solution \mathbf{b}^* to step 4 of Algorithm 2

- 1: **for** $k = 0, 1, \dots, K_{\max}$ **do**
- 2: Compute the gradient, $\mathbf{g}^k = \nabla f_{\text{row}}(\mathbf{b}^k)$, using $\hat{\mathbf{x}}$ and $\mathbf{\Pi}$ in (3.1)
- 3: Compute the first-order KKT violation

$$\text{kkt}_{\text{viol}} = \text{sqrt} \left(\sum_r [\min\{b_r^k, g_r^k\}]^2 \right)$$

- 4: **if** $\text{kkt}_{\text{viol}} \leq \tau$ **then**
- 5: **return** $\mathbf{b}^* = \mathbf{b}^k$ ▷ Converged to tolerance.
- 6: **end if**
- 7: Find the indices of free variables from (3.3) with $\epsilon = 10^{-3}$ in (3.2)
- 8: Calculate the Hessian for free variables

$$\mathbf{H}_F^k = [\nabla^2 f_{\text{row}}(\mathbf{b}^k)]_{\mathcal{F}}$$

- 9: Compute the damped Newton direction $\mathbf{d}_F^k = -(\mathbf{H}_F^k + \mu_k I)^{-1} \mathbf{g}_F^k$
- 10: Construct search direction \mathbf{d}^k over all variables using \mathbf{d}_F^k and \mathbf{g}^k in (3.5)
- 11: Perform the projected line search (3.8) using σ and β to find step length α_k
- 12: Update the current iterate

$$\mathbf{b}^{k+1} = P_+[\mathbf{b}^k + \alpha_k \mathbf{d}^k]$$

- 13: Update the damping parameter μ_{k+1} according to (3.6)-(3.7)
 - 14: **end for**
 - 15: **return** $\mathbf{b}^* = \mathbf{b}^k$ ▷ Iteration limit reached.
-

threshold in PDN-R from (3.2) was set to $\epsilon = 10^{-3}$. The L-BFGS approximations in PQN-R stored the 3 most recent update pairs (3.9).

The multiplicative update algorithm that we compare with is that of Chi and Kolda [10], available as function `cp_apr` in the Matlab Tensor Toolbox [5], and called MU in this section. It builds on tensor generalizations of the Lee and Seung method, specifically treating *inadmissible zeros* (their term for factor elements that are active but close to zero) to improve the convergence rate. Algorithm MU can be tuned by selecting the number of inner iterations for approximately solving the subproblem at step 5 of Algorithm 1. We found that 10 inner iterations worked well in all experiments.

We also compare to a projected quasi-Newton algorithm adopted from Kim et al. [20], called PQN in this section. PQN is similar to PQN-R but solves (2.4) without reformulating the block subproblem into row subproblems. Like PQN-R, PQN identifies the active set using $\epsilon = 0$ in (3.2), and maintains a limited memory BFGS approximation of the Hessian. However, PQN uses one L-BFGS matrix for the entire subproblem, storing the 3 most recent update pairs. We used Matlab code from the authors of [20], embedding it in the alternating framework of Algorithm 1, with the modifications described in section 3.2.

We compare PDN-R to a similar damped Hessian method that uses one matrix for the block subproblem instead of a matrix for every row subproblem. We call this

Algorithm 4 Projected Quasi-Newton Solver PQN-R for the Row Subproblem

Given data $\hat{\mathbf{x}}$ and $\mathbf{\Pi}$, constants $\mu_0, \sigma, \beta, K_{\max}$, stop tolerance τ , and initial values \mathbf{b}^0
Return a solution \mathbf{b}^* to step 4 of Algorithm 2

- 1: **for** $k = 0, 1, \dots, K_{\max}$ **do**
- 2: Compute the gradient, $\mathbf{g}^k = \nabla f_{\text{row}}(\mathbf{b}^k)$, using $\hat{\mathbf{x}}$ and $\mathbf{\Pi}$ in (3.1)
- 3: Compute the first-order KKT violation

$$\text{kkt}_{\text{viol}} = \text{sqrt} \left(\sum_r [\min\{b_r^k, g_r^k\}]^2 \right)$$

- 4: **if** $\text{kkt}_{\text{viol}} \leq \tau$ **then**
- 5: **return** $\mathbf{b}^* = \mathbf{b}^k$ ▷ Converged to tolerance.
- 6: **end if**
- 7: Find the indices of free variables from (3.3) with $\epsilon = 0$ in (3.2)
- 8: Construct search direction \mathbf{d}^k using \mathbf{g}^k in (3.10)
- 9: Perform the projected line search (3.8) using σ and β to find step length α_k
- 10: Update the current iterate

$$\mathbf{b}^{k+1} = P_+[\mathbf{b}^k + \alpha_k \mathbf{d}^k]$$

- 11: Update the L-BFGS approximation with \mathbf{b}^{k+1} and \mathbf{g}^{k+1}
 - 12: **end for**
 - 13: **return** $\mathbf{b}^* = \mathbf{b}^k$ ▷ Iteration limit reached.
-

method PDN. It exploits the block diagonal nature of the Hessian to construct a search direction for the same computational cost as PDN-R; i.e., one search direction of PDN takes the same effort as computing one search direction for all row subproblems in PDN-R. Similar remarks apply to computation of the objective function for the subproblem (2.4). However, PDN applies a single damping parameter μ_k to the block subproblem Hessian, and updates all variables in the block subproblem from a single line search along the search direction.

All algorithms were coded in Matlab using the sparse tensor objects of the Tensor Toolbox [5]. All experiments were performed on a Linux workstation with 12GB memory. Data sets were large enough to be demanding but small enough to fit in machine memory; hence, performance results are not biased by disk access issues.

The experiments that follow show three important results:

1. The row subproblem formulation is better suited to second order methods than a block subproblem formulation.
2. PDN-R and PQN-R have a faster convergence rate than the other algorithms in reducing the kkt_{viol} , especially when solving to high accuracy. This holds for all problem sizes.
3. PDN-R and PQN-R reach good solutions with high sparsity more quickly than the other algorithms, a desirable feature when the factor matrices are expected to be sparse.

In section 4.1 we report on algorithmic performance in solving the block subproblem (2.4), since the time is representative of the total time it will take to solve the full tensor factorization problem (2.1). In section 4.2 we report results from solving the full problem within the alternating block framework (Algorithm 1).

4.1. Solving the Convex Block Subproblem. We begin by examining algorithm performance on the convex subproblem (2.4) of the alternating block framework. As algorithms iterate through alternating modes of the tensor, subproblems of different shapes are solved; here we look at a single representative subproblem. Our goal is to characterize the relative behavior of algorithms on the representative block subproblem.

Appendix A describes our method for generating synthetic test problems with reasonable sparsity. We investigate a 3-way tensor of size $200 \times 300 \times 400$, generating $S = 500,000$ data samples. The number of components, R , is varied over the set $\{20, 40, 60, 80, 100\}$. For each value of R , the procedure generates a sparse multilinear model $\mathcal{M} = \llbracket \boldsymbol{\lambda}; \mathbf{A}^{(1)}, \mathbf{A}^{(2)}, \mathbf{A}^{(3)} \rrbracket$ and data tensor \mathcal{X} . Table 4.1 lists the number of nonzero elements found in the data tensor \mathcal{X} that results from 500,000 data samples.

Table 4.1: Subproblem sparsity for number of components R

R	NUMBER NONZEROS	DENSITY
20	408,053	1.70%
40	450,217	1.88%
60	465,086	1.94%
80	471,079	1.96%
100	475,025	1.98%

We consider just the subproblem obtained by unfolding along mode 1; hence, the test case will contain 200 row subproblems of the form (2.6). To solve just the mode 1 subproblem, the for loop at step 3 of Algorithm 1 is changed to $n = 1$.

We will run several trials of the subproblem solver from different initial guesses of the unknowns, holding $\mathbf{A}^{(2)}$ and $\mathbf{A}^{(3)}$ from \mathcal{M} constant. The initial guess draws each element of $\mathbf{A}^{(1)}$ from a uniform distribution on $[0, 1)$ and sets each element of $\boldsymbol{\Lambda}$ to one. To satisfy constraints in (2.1), the columns of $\mathbf{A}^{(1)}$ are normalized and the normalization factor is absorbed into $\boldsymbol{\Lambda}$. The mode 1 subproblem (2.4) is now defined with $\boldsymbol{\Pi} = (\mathbf{A}^{(3)} \odot \mathbf{A}^{(2)})^T$, $\mathbf{X} = \mathbf{X}_{(1)}$, and $\mathbf{B} = \mathbf{A}^{(1)}\boldsymbol{\Lambda}$, with unknowns \mathbf{B} initialized as described.

4.1.1. PDN-R and PDN on the Convex Subproblem. We first characterize the behavior of our Newton-based algorithm, PDN-R, and compare it with PDN. Row subproblems were solved using Algorithm 3 with stop tolerance $\tau = 10^{-8}$ and the parameter values mentioned at the beginning of section 4. The value of K_{\max} in Algorithm 3 was large enough that the kkt_{viol} converged to τ before K_{\max} was reached.

Figures 4.1a, 4.1b, and 4.1c show how KKT violations decrease with iteration for three different values of R . The subproblem was solved 10 times from different randomly chosen start points. (Since the subproblem is strictly convex, there is a single unique minimum that is reached from every start point.) Each solid line plots the maximum kkt_{viol} over all 200 row subproblems for one of the 10 PDN-R runs. Each dashed line plots the kkt_{viol} of the block subproblem for one of the 10 PDN runs. Note the y -axis is the \log_{10} of kkt_{viol} . The figure demonstrates that after some initial slow progress, both algorithms exhibit the fast quadratic convergence rate typical of Newton methods. PDN-R clearly takes fewer iterations to compute a factorization with small kkt_{viol} .

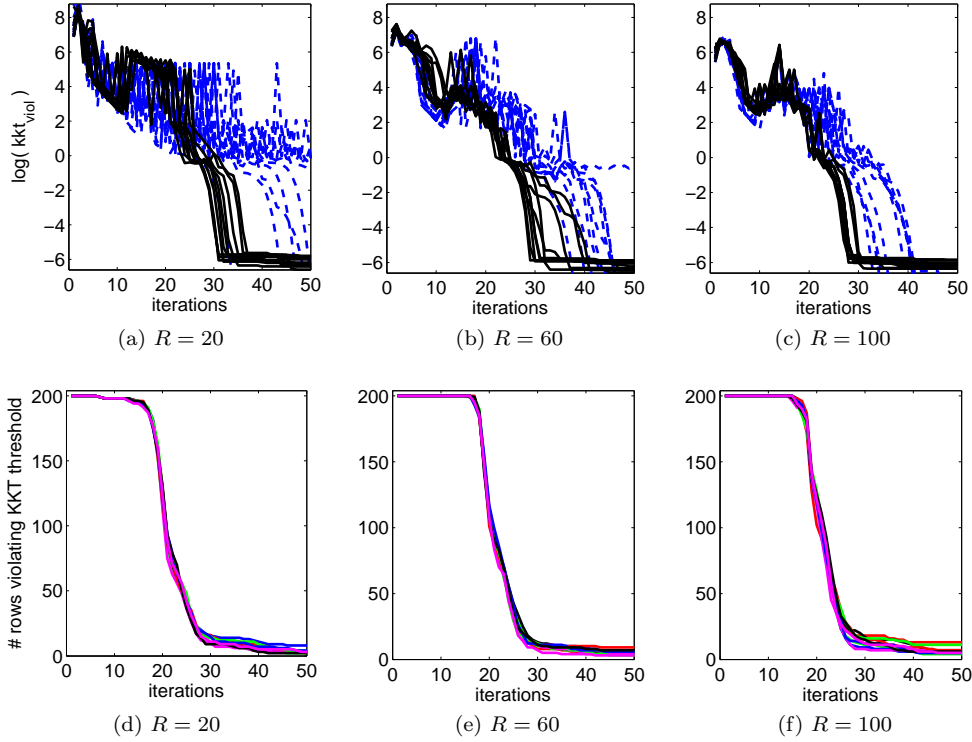


Fig. 4.1: Convergence behavior of PDN-R (Algorithm 3) and PDN over 10 runs with different start points, for three values of R . The upper graphs plot $\log(\text{kkt}_{\text{viol}})$, showing how the maximum violation over all row subproblems varies as the number of iterations increases. Solid lines are PDN-R, dashed lines are PDN. The lower graphs plot the number of rows violating the KKT-based stop tolerance (PDN-R only).

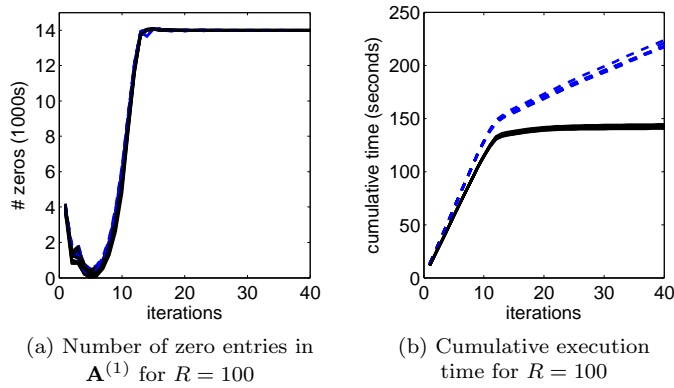


Fig. 4.2: Additional convergence behavior over 10 runs with different start points. Solid lines are PDN-R, dashed lines are PDN.

Figures 4.1d, 4.1e, and 4.1f show the number of row subproblems that satisfy the KKT-based stop tolerance after a given number of iterations. Remember that *all* row subproblems must satisfy the KKT tolerance before the algorithm declares a solution.

Figure 4.2 shows additional features of the convergence, for just the case of $R = 100$ components (behavior is similar for other values of R). In Figure 4.2a we see the number of elements of $\mathbf{A}^{(1)}$ exactly equal to zero. Data for this experiment was generated from a sparse K-tensor plus noise (see Appendix A); hence, we expect a sparse solution. The plot indicates that sparsity can be achieved after reducing kkt_{viol} to a moderately small tolerance (around 10^2 in this example). We will return to sparsity of the solution in the sections below.

In Figure 4.2b we see that execution time per iteration decreases when variables are closer to a solution. PDN-R execution time becomes very small because only a few row subproblems need to satisfy the convergence tolerance. PDN takes more time per iteration because it must compute a search direction for the entire block subproblem. These experiments show that PDN-R and PDN behave similarly for the convex subproblem and that PDN-R is a little faster; much larger differences will appear when the full factorization is computed in section 4.2.1.

4.1.2. PQN-R and PQN on the Convex Subproblem. In this section we demonstrate the importance of the row subproblem formulation by comparing PQN-R with PQN, demonstrating the huge speedup achieved with our row subproblem formulation. We compare the algorithms on the mode 1 subproblem described above, from the same 10 random initial guesses for $\mathbf{A}^{(1)}$. Table 4.2 lists the average CPU times over 10 runs. PQN-R was executed until the kkt_{viol} was less than $\tau = 10^{-8}$. PQN was unable to achieve this level of accuracy, so execution was stopped at a tolerance of 10^{-3} . Results in the table show that PQN-R is much faster at decreasing the KKT violation. We note that a KKT violation of 10^{-8} is approximately the square root of machine epsilon, the smallest practical value that can be attained.

Table 4.2: Convergence comparison in solving the subproblem

R	Algorithm PQN		Algorithm PQN-R	
	$\text{kkt}_{\text{viol}} < 10^{-1}$	$\text{kkt}_{\text{viol}} < 10^{-3}$	$\text{kkt}_{\text{viol}} < 10^{-1}$	$\text{kkt}_{\text{viol}} < 10^{-8}$
20	625 secs	690 secs	12.4 secs	17.1 secs
40	755 secs	846 secs	10.9 secs	16.4 secs
60	822 secs	920 secs	11.3 secs	16.8 secs
80	1022 secs	1141 secs	13.7 secs	19.5 secs
100	993 secs	1125 secs	13.1 secs	20.2 secs

The two algorithms also differ in how they discover the number of elements in $\mathbf{A}^{(1)}$ equal to zero. Both eventually agree on the number of zero elements, but PQN-R is much faster. Figure 4.3 shows the progress made by the two algorithms; the behavior of PQN for this quantity is erratic and slow to converge.

Algorithm PQN might be relatively more competitive for tensor subproblems with a small number of rows, but many applications are of the size we consider in at least one tensor mode. It is apparent that applying L-BFGS to the block subproblem does not work as well as applying separate instances of L-BFGS to the row subproblems. This is not surprising since the first method ignores the block diagonal structure of the true Hessian. We see no advantages to using PQN and do not consider it further.

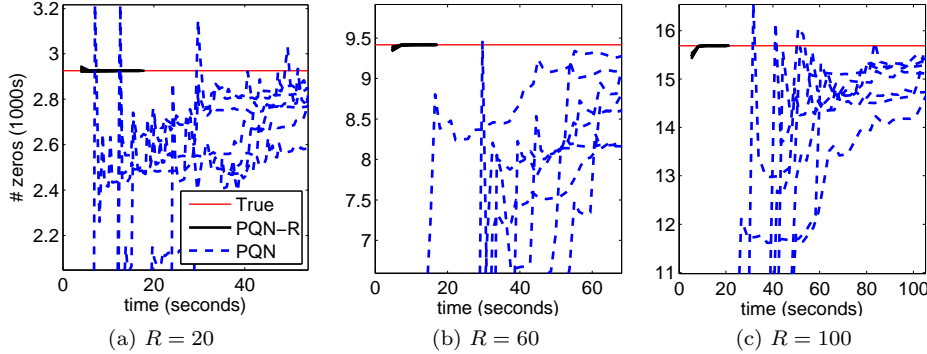


Fig. 4.3: Number of elements equal to zero in $\mathbf{A}^{(1)}$ found by PQN-R (solid lines, forming a short segment in the upper left) and PQN (dashed lines) as a function of compute time, for a subproblem with different values of R . The same subproblem was solved from six different start points, corresponding to the different colors. The red horizontal line shows the true value.

4.1.3. PDN-R, PQN-R, and MU on the Convex Subproblem. Next we compare our new row-based algorithms, PDN-R and PQN-R, with the multiplicative update method MU [10]. Again we use the mode 1 subproblem of section 4.1, from the same 10 random initial guesses.

As described in section 4, MU is a state of the art representative of the most common algorithm for nonnegative tensor factorization. It is a form of scaled steepest descent with bound constraints [26], and therefore is expected to converge more slowly than Newton or quasi-Newton methods. We see this clearly in Table 4.3 for two different stop tolerances. The MU algorithm was executed with a time limit of 1800 seconds per problem, and failed to reach $\text{kkt}_{\text{viol}} < 10^{-3}$ before this limit when R was 60 or larger.

Table 4.3: Time to reach stop tolerance for 3 algorithms (averaged over 10 runs)

R	$\text{kkt}_{\text{viol}} = 10^{-2}$			$\text{kkt}_{\text{viol}} = 10^{-3}$		
	PDN-R	PQN-R	MU	PDN-R	PQN-R	MU
20	8.1 secs	14.5 secs	97.7 secs	8.1 secs	15.6 secs	161.3 secs
40	25.1 secs	13.1 secs	239.2 secs	25.2 secs	14.6 secs	485.9 secs
60	53.6 secs	13.8 secs	469.2 secs	53.7 secs	15.6 secs	>1800 secs
80	92.8 secs	16.3 secs	455.4 secs	92.9 secs	18.1 secs	>1800 secs
100	139.8 secs	16.0 secs	730.7 secs	140.0 secs	18.3 secs	>1800 secs

Of course, the disparity in convergence time is more pronounced when a smaller KKT error is demanded. Figure 4.4 shows the decrease in KKT violation as a function of compute time. Here we see that MU makes a faster initial reduction in KKT violation than PDN-R or PQN-R, but then it slows to a linear rate of convergence. Notice the gap from time zero for PDN-R and PQN-R, which reflects setup cost before the first iteration result is computed. For PQN-R the setup time is fairly constant with R (about 3.8 seconds), while PDN-R has a setup time that increases with R (11.5

seconds for $R = 100$). Unlike MU, both algorithms must construct software structures for all row subproblems before a first iteration result appears. Figure 4.4 also reveals that PDN-R is slower relative to PQN-R as the number of factors R increases. This is because the cost of solving a Newton-based Hessian is $O(R^2)$, while the limited memory BFGS Hessian cost is $O(R)$.

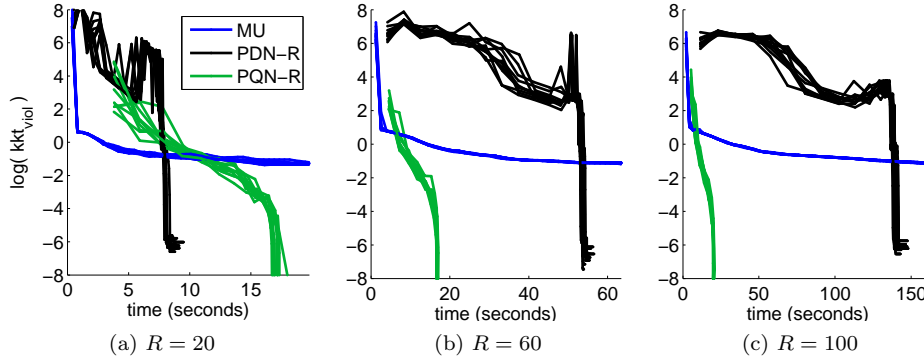


Fig. 4.4: Convergence behavior comparison on subproblem for different values of R (10 runs each). Algorithm MU (blue) makes fast initial progress in reducing the violation, but slows dramatically after reaching a violation of about 0.1. PDN-R (black) and PQN-R (green) reduce the violation much further, with PQN-R being faster for higher values of R .

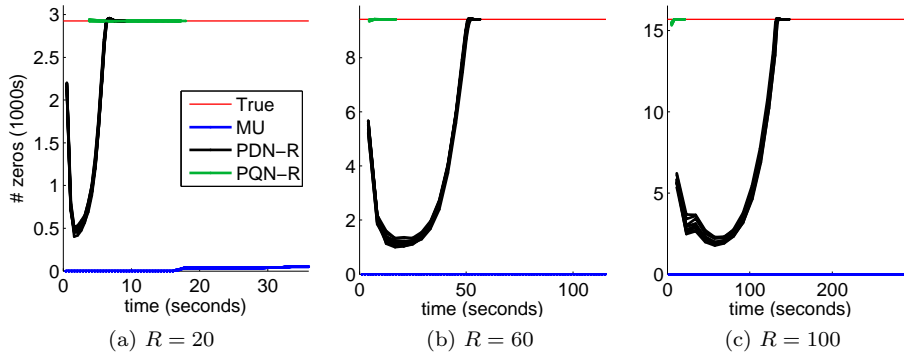


Fig. 4.5: Effectiveness of the 3 algorithms in finding a sparse solution for different values of R . In each case the number of elements in $\mathbf{A}^{(1)}$ equal to zero is plotted against execution time. The PDN-R (black) and PQN-R (green) algorithms are much faster than MU (blue) at finding the zeros. The horizontal red line shows the true value.

Figure 4.4 indicates that algorithm MU is preferred if a relatively large kkt_{viol} is acceptable. We argue that this is *not* acceptable if the goal is to find a sparse solution. Figure 4.5 plots the number of elements that equal zero as a function of CPU time.

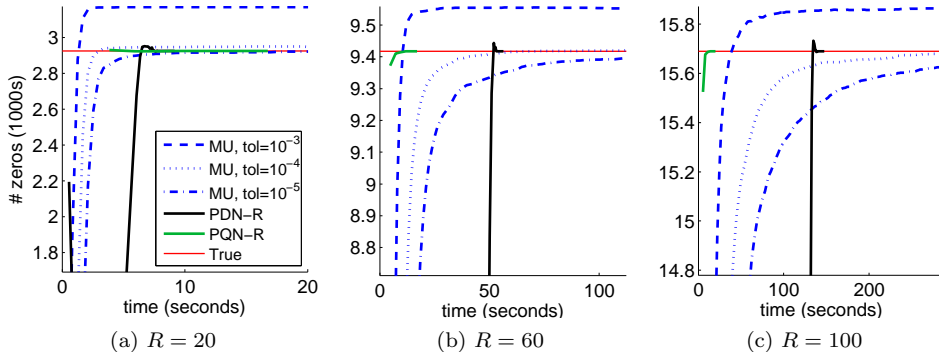


Fig. 4.6: Comparison of PDN-R, PQN-R and MU in finding elements of $\mathbf{A}^{(1)}$ equal to zero for a sample run. MU rarely finds exact zeros; therefore, we show results of applying various thresholds. Some experimentation may be needed to find the best threshold; regardless, it is slower than the methods proposed here.

It shows that PDN-R and PQN-R both converge to the correct number much faster than MU.

On closer inspection we see that MU is actually making factor elements small, and is just very slow at making them exactly zero. If we choose a small positive threshold instead of zero, then MU might arguably do well at finding a sparse solution. Figure 4.6 summarizes an investigation of this idea. Three different thresholds are shown: 10^{-3} , 10^{-4} , and 10^{-5} . The first threshold is clearly too large, declaring elements to be “zero” when they never converge to such a value. A threshold of 10^{-4} is also too large for $R = 20$, though possibly acceptable for $R = 40$ and $R = 60$. The choice of 10^{-5} correctly identifies elements converging to zero, but PDN-R and PQN-R identifies them much faster. We conclude that PDN-R and PQN-R are significantly better at finding a true sparse solution than MU, in terms of robustness (no need to choose an ad-hoc threshold) and computation time (assuming a suitable threshold for MU is known).

4.2. Solving the Full Problem. In this section we move from a convex subproblem to solving the full factorization (2.1). We generate the same $200 \times 300 \times 400$ tensor data as in section 4.1, and now treat all modes as optimization variables. An initial guess is constructed for all three modes in the same manner that $\mathbf{A}^{(1)}$ was initialized in section 4.1. We generate 10 different tensors by changing the random seed used in Algorithm 5, and solve each from a single initial guess. All solvers used the same initial guess; however, since the full factorization is a nonconvex optimization problem, algorithms may converge to different local solutions.

We expect our local solutions to be reasonably close to the multilinear model $\mathcal{M} = [\boldsymbol{\lambda}; \mathbf{A}^{(1)}, \dots, \mathbf{A}^{(N)}]$ that generated the synthetic tensor data. We compared computed solutions with the original K-tensor model using the Tensor Toolbox function `score` with option `greedy`. This function considers all factor matrices and weights, producing a number between zero (poor match) and one (exact match) [2]. K-tensor solutions computed with PDN-R to a tolerance of $\tau = 10^{-4}$ scored above 0.90. (Scores of less than 0.02 resulted when comparing the K-tensor solution of PDN-R to other models generated with a different random seed.) These results show that an accurate

factorization can yield the original factors for our test problems; however, our focus is on behavior of the algorithms in computing a solution.

4.2.1. Comparing PDN-R with PDN. We first compare the two Newton-based methods: PDN-R, which solves row subproblems for each tensor mode, and PDN, which instead solves the block subproblem as a single matrix. In section 4.1.1 we saw that the two methods behaved similarly for the convex subproblem of a single tensor mode (except that PDN-R was faster). However, on the full factorization PDN is often unable to make progress from a start point where the KKT violation is large. Sometimes the search direction does not satisfy the sufficient decrease condition of the Armijo line search, even after 10 back-tracking iterations. More frequently, the line search puts too many variables at the bound of zero, causing the objective function to become undefined in equation (2.4) because $\mathbf{B}^{(n)}\mathbf{\Pi}^{(n)}$ is zero for elements where $\mathbf{X}_{(n)}$ is nonzero.

If the line search fails in a subproblem, then we compute a multiplicative update step for that iteration to make progress. This allows PDN to reach points where the KKT error is smaller, and we find that subsequent damped Newton steps are successful until convergence. Table 4.4 quantifies the number of line search failures over the first 20 iterations, beginning from a random start point where kkt_{viol} is typically larger than 10^3 . Columns in the table correspond to different values for the initial damping parameter μ_0 . We expect larger values of μ_k to improve robustness by effectively shortening the step length and hopefully avoiding the mistake of setting too many variables to zero. (A serious drawback to increasing μ_k is that it damps out Hessian information, which can hinder the convergence rate.) The table shows that improvement in robustness is made; however, PDN still suffers from some line search failures. In contrast, PDN-R does not have any line search failures for the same test problems and start points, using the default $\mu_0 = 10^{-5}$.

Table 4.4: Line search failures by PDN in the first 20 iterations, averaged over 5 runs. There were up to 900 possible line searches in each case (a maximum of 15 inner iterations per mode, over 20 outer iterations).

R	$\mu_0 = 10^1$	$\mu_0 = 10^{-2}$	$\mu_0 = 10^{-5}$
20	57.8	88.4	142.2
40	76.2	87.4	164.6
60	59.0	90.8	201.0
80	41.4	82.8	184.6
100	28.8	62.2	168.0

Table 4.5 shows that PDN-R is significantly faster than PDN even in the region where PDN operates robustly. These runs began at a start point where $\text{kkt}_{\text{viol}} < 0.1$ so that PDN did not suffer any line search failures. 5 runs were made for each of the 5 values of R , and results compared at the iteration where an algorithm reduced kkt_{viol} below a given threshold (rows of Table 4.5). PDN did not always reach a threshold value in the three hour computation time limit. The third column shows that the number of outer iterations needed to reach a threshold was very similar between PDN-R and PDN. The fourth column shows that PDN-R executed much faster.

Iterations of PDN-R run faster because each row subproblem has an individualized step size and damping parameter (this was discussed previously in section 4.1.1).

Table 4.5: Comparison of PDN-R and PDN execution times for various stop tolerances. 25 experiments were run, the algorithms compared for each experiment that PDN completed, and the average value reported. The fourth column shows that PDN-R executes from 8 to 9 times faster than PDN (the column reports average and standard deviation).

kkt_{viol}	PDN successes	avg diff in outer its	avg speedup of PDN-R
10^{-2}	23	2.48 %	9.1 ± 1.4
10^{-3}	20	3.02 %	8.7 ± 1.4
10^{-4}	16	2.68 %	8.5 ± 1.7
10^{-5}	12	7.93 %	9.5 ± 2.4

Given the large disparity in execution time and the lack of robustness when far from a solution, we find no advantages to using PDN and do not consider it further.

4.2.2. Comparing PDN-R, PQN-R, and MU. Table 4.6 summarizes the time taken to reach a KKT threshold of 10^{-3} for each algorithm over the synthetic data tensors. Like the convex subproblem tested in section 4.1.3, the PDN-R and PQN-R methods converge to this relatively high accuracy much faster than MU, again showing the value of second-order information. As in the subproblem, we see that PQN-R is faster relative to PDN-R as the number of factors R increases. Figure 4.7 shows convergence behavior of the full factorization problem in the same way that Figure 4.4 showed behavior of the convex subproblem. The KKT error of the full problem does not reach the quadratic rate of decrease seen in the subproblem. This is due to nonconvexity of the full factorization problem, and the alternation between solutions of each mode.

Table 4.6: Time to reach stop tolerance 10^{-3} on full problem (over 10 runs). Mean and standard deviation are reported. Some runs of MU failed to reach the tolerance in 1000 iterations.

R	PDN-R	PQN-R	MU
20	467 ± 208 secs	485 ± 189 secs	912 ± 412 secs (0 failures)
40	819 ± 295 secs	961 ± 504 secs	1666 ± 501 secs (2 failures)
60	1270 ± 506 secs	1300 ± 515 secs	2192 ± 357 secs (5 failures)
80	1359 ± 306 secs	832 ± 167 secs	2634 ± 559 secs (1 failure)
100	1860 ± 338 secs	959 ± 237 secs	3620 ± 1018 secs (1 failure)

As with the subproblem, we also observe better convergence by our methods to a sparse solution. Figure 4.8 shows PDN-R and PQN-R reaching the final count of zero elements much faster than MU. As in section 4.1.3, we argue that PDN-R and PQN-R are superior when the task is to find a solution with correct sparsity.

4.2.3. Comparing with DBLP Data. We also ran the same three algorithms on the sparse 3-way tensor of DBLP data [13] examined in [15]. The data counts the number of papers published by author i_1 at conference i_2 in year i_3 , with dimensions $7108 \times 1103 \times 10$. The tensor contains 112,730 nonzero elements, a density of 0.14%. The data was factorized for R between 10 and 100 in [15] (using a least squares objective function), so we use $R \in \{20, 60, 100\}$ in our experiments. Behavior of the algorithms on the DBLP data was similar to behavior on our synthetic data.

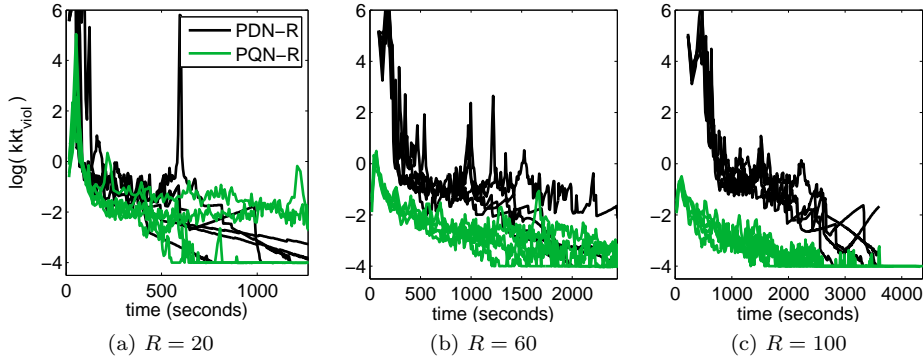


Fig. 4.7: Convergence behavior of the PDN-R (black lines) and PQN-R (green lines) algorithms in computing a full 3-way solution. Each algorithm was run from 10 variants of the tensor data.

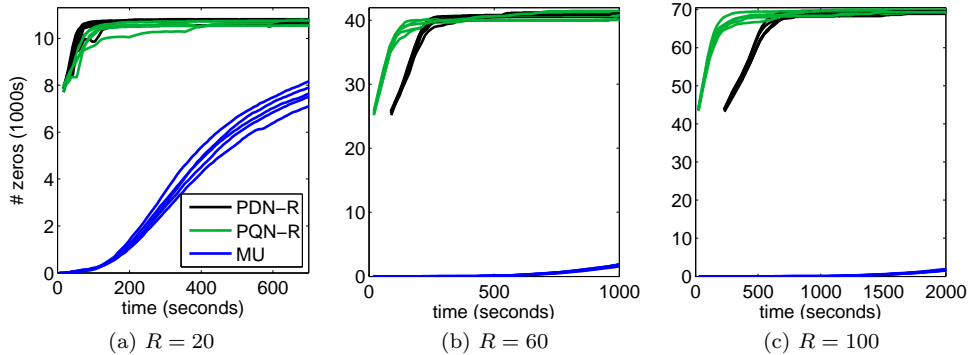


Fig. 4.8: Effectiveness of the algorithms in finding a sparse solution for a full 3-way solution. In each case the total number of elements in $\mathbf{A}^{(1)}$, $\mathbf{A}^{(2)}$, and $\mathbf{A}^{(3)}$ equal to zero is plotted against execution time. The PDN-R (black lines) and PQN-R (green) algorithms are much faster than MU (blue). Each algorithm was run with 10 variants of the tensor data, so the final number of zero elements is different in each case.

Figure 4.9 shows how the count of elements equal to zero changes as algorithms progress, for 10 runs that start from different random initial guesses. Again we see that PDN-R and PQN-R reach a sparse solution faster than MU.

Factorizations of the DBLP data computed with PDN-R and PQN-R were quite sparse, making them easier to interpret. The fraction of elements exactly equal to zero in the computed conference factor matrix was 98.1%. The author factor matrix was also very sparse, with 95.4% of the elements exactly zero. These results were for a factorization with $R = 100$, stopped after 800 seconds of execution with the KKT violation reduced to around 5×10^{-4} . Figure 4.10 shows a component that detects related conferences that took place only in even years. The two dominant conferences are the same as those reported in Figure 7 of [15]. Figure 4.11 shows

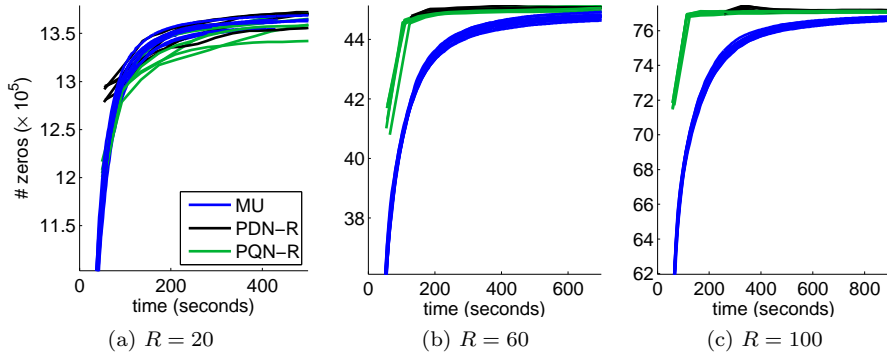


Fig. 4.9: Effectiveness of the algorithms in finding a sparse solution for the DBLP tensor. In each case the total number of elements in $\mathbf{A}^{(1)}$, $\mathbf{A}^{(2)}$, and $\mathbf{A}^{(3)}$ equal to zero is plotted against execution time. The PDN-R (black lines) and PQN-R (green) algorithms are much faster than MU (blue).

another component that groups conferences that took place only in odd years. In both components the sparsity is striking, especially for the conference factor.

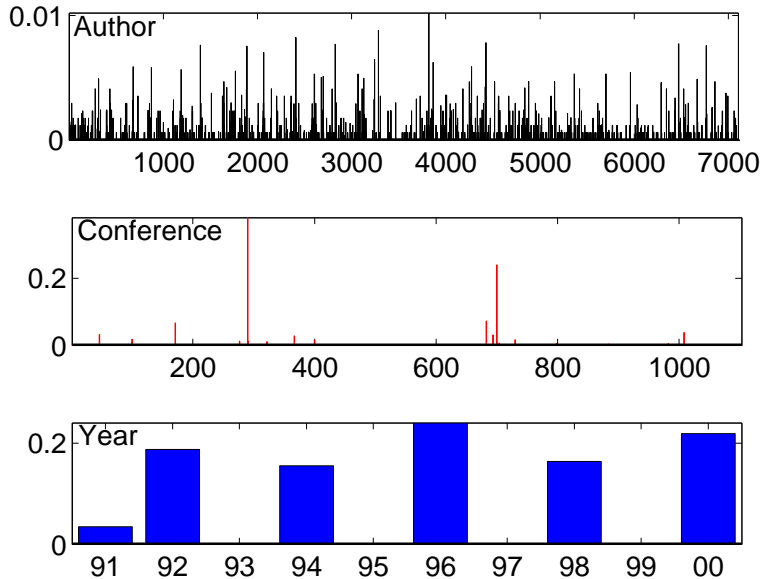


Fig. 4.10: Computed factors from DBLP data for component 26 (i.e., the 26-th largest component by weight). The two dominant conferences, ECAI and KR, occurred only in even years, except for KR in 1991. 91% (6456) of elements in the author factor are exactly zero, as are 98% (1084) conference elements.

5. Summary. In this paper we derived a *row subproblem* formulation for non-negative tensor factorization of the Kullback-Leibler objective that allows efficient use

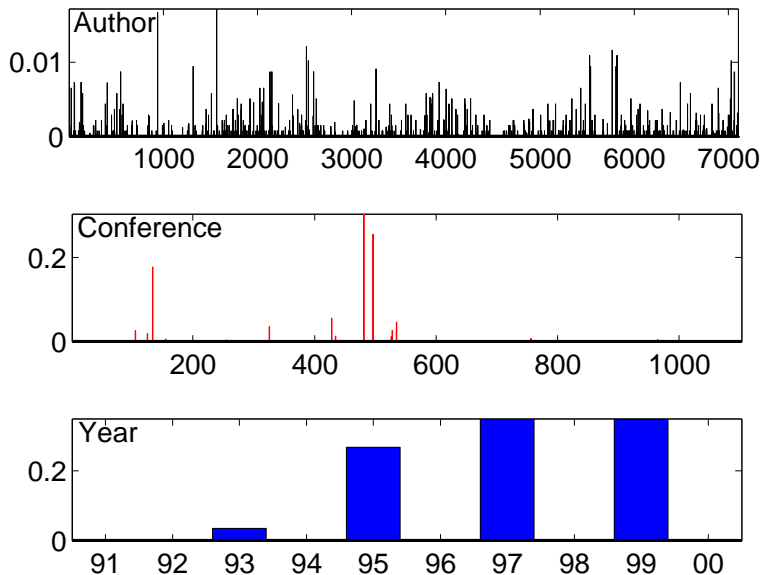


Fig. 4.11: Computed factors from DBLP data for component 41. The three dominant conferences (ICDAR, ICIAP, and CAIP) occurred only in odd years. 93% (6626) of elements in the author factor are exactly zero, as are 98% (1083) conference elements.

of second order information. We wrote and tested two new algorithms that exploit the row subproblem reformulation: PDN-R uses second derivatives in the optimization, while PQN-R uses a quasi-Newton approximation. We showed that using the same second order information in a block subproblem formulation is less robust and more expensive computationally than a row subproblem formulation. We showed that both PDN-R and PQN-R are much faster than the best multiplicative update method when high accuracy solutions are desired. We further showed that high accuracy is needed to identify zeros and compute sparse factors without resorting to the use of ad-hoc thresholds. This is important because sparse count data is likely to have sparsity in the factors, and sparse factors are always easier to interpret.

Our Matlab algorithms will appear in the next release of the Tensor Toolbox [5]. We mentioned in section 2.1 that row subproblems can be solved in parallel, and we anticipate developing other versions of the algorithms for shared and distributed memory machines.

Acknowledgments. We thank the authors of [20] for sharing Matlab code that we used in the experiments.

This work was partially funded by the Laboratory Directed Research & Development (LDRD) program at Sandia National Laboratories. Sandia National Laboratories is a multiprogram laboratory operated by Sandia Corporation, a wholly owned subsidiary of Lockheed Martin Corporation, for the United States Department of Energy's National Nuclear Security Administration under contract DE-AC04-94AL85000.

- [1] E. ACAR, D. M. DUNLAVY, AND T. G. KOLDA, *A scalable optimization approach for fitting canonical tensor decompositions*, Journal of Chemometrics, 25 (2011), pp. 67–86.
- [2] E. ACAR, T. G. KOLDA, AND D. M. DUNLAVY, *All-at-once optimization for coupled matrix and tensor factorizations*, in KDD Workshop Proceedings for the 9th Workshop on Mining and Learning with Graphs, 2011.
- [3] G. ANDREW AND J. GAO, *Scalable training of l_1 -regularized log-linear models*, in Proceedings of the 24th International Conference on Machine Learning, ACM, 2007, pp. 33–40.
- [4] B. W. BADER, M. W. BERRY, AND M. BROWNE, *Discussion tracking in Enron email using PARAFAC*, in Survey of Text Mining: Clustering, Classification, and Retrieval, M. W. Berry and M. Castellanos, eds., Springer, 2nd ed., 2007, ch. 8, pp. 147–162.
- [5] B. W. BADER, T. G. KOLDA, ET AL., *MATLAB Tensor Toolbox version 2.5*. Available online, January 2012. <http://www.sandia.gov/~tgkolda/TensorToolbox/>.
- [6] D. BERTSEKAS, *On the Goldstein-Levitin-Polyak gradient projection method*, IEEE Transactions on Automatic Control, 21 (1976), pp. 174–184.
- [7] D. BERTSEKAS, *Projected newton methods for optimization problems with simple constraints*, SIAM Journal on Control and Optimization, 20 (1982), pp. 221–246.
- [8] R. BRO AND S. D. JONG, *A fast non-negativity-constrained least squares algorithm*, Journal of Chemometrics, 11 (1997), pp. 393–401.
- [9] J. D. CARROLL AND J. J. CHANG, *Analysis of individual differences in multidimensional scaling via an N -way generalization of ‘Eckart-Young’ decomposition*, Psychometrika, 35 (1970), pp. 283–319.
- [10] E. C. CHI AND T. G. KOLDA, *On tensors, sparsity, and nonnegative factorizations*, SIAM Journal on Matrix Analysis and Applications, 33 (2012), pp. 1272–1299.
- [11] A. CICHOCKI AND A.-H. PHAN, *Fast local algorithms for large scale nonnegative matrix and tensor factorizations*, IEICE Transactions on Fundamentals of Electronics, Communications and Computer Sciences, 92 (2009), pp. 708–721.
- [12] A. CONN, N. GOULD, AND P. TOINT, *Global convergence of a class of trust region algorithms for optimization with simple bounds*, SIAM Journal on Numerical Analysis, 25 (1988), pp. 433–460.
- [13] *DBLP data*, 2011. <http://www.informatik.uni-trier.de/~ley/db/>.
- [14] I. S. DHILLON AND S. SRA, *Generalized nonnegative matrix approximations with Bregman divergences*, in Neural Information Proc. Systems (NIPS), 2005, pp. 283–290.
- [15] D. M. DUNLAVY, T. G. KOLDA, AND E. ACAR, *Temporal link prediction using tensor and matrix factorizations*, ACM Transactions on Knowledge Discovery from Data, 5 (2011).
- [16] M. P. FRIEDLANDER AND K. HATZ, *Computing nonnegative tensor factorizations*, Computational Optimization and Applications, 23 (2008), pp. 631–647.
- [17] E. GONZALEZ AND Y. ZHANG, *Accelerating the Lee-Seung algorithm for non-negative matrix factorization*, Tech. Report TR-05-02, Department of Computational and Applied Mathematics, Rice University, Houston, TX, 2005.
- [18] R. A. HARSHMAN, *Foundations of the PARAFAC procedure: Models and conditions for an “explanatory” multi-modal factor analysis*, UCLA Working Papers in Phonetics, 16 (1970). Available online, <http://publish.uwo.ca/~harshman/wpppfac0.pdf>.
- [19] C.-J. HSIEH AND I. S. DHILLON, *Fast coordinate descent methods with variable selection for non-negative matrix factorization*, in Proceedings of the 17th ACM SIGKDD International Conference on Knowledge Discovery and Data Mining, ACM, 2011, pp. 1064–1072.
- [20] D. KIM, S. SRA, AND I. DHILLON, *Tackling box-constrained optimization via a new projected quasi-Newton approach*, SIAM Journal on Scientific Computing, 32 (2010), pp. 3548–3563.
- [21] D. KIM, S. SRA, AND I. S. DHILLON, *Fast projection-based methods for the least squares non-negative matrix approximation problem*, Statistical Analysis and Data Mining, 1 (2008), pp. 38–51.
- [22] H. KIM AND H. PARK, *Nonnegative matrix factorization based on alternating nonnegativity constrained least squares and active set method*, SIAM Journal on Matrix Analysis and Applications, 30 (2008), pp. 713–730.
- [23] J. KIM AND H. PARK, *Fast nonnegative tensor factorization with an active-set-like method*, in High-Performance Scientific Computing, Algorithms and Applications, M. W. Berry, K. A. Gallivan, E. Gallopoulos, A. Grama, B. Philippe, Y. Saad, and F. Saied, eds., Springer, 2012, pp. 311–326.
- [24] T. G. KOLDA AND B. W. BADER, *Tensor decompositions and applications*, SIAM Review, 51 (2009), pp. 455–500.
- [25] D. D. LEE AND H. S. SEUNG, *Learning the parts of objects by non-negative matrix factorization*, Nature, 401 (1999), pp. 788–791.
- [26] ———, *Algorithms for non-negative matrix factorization*, Advances in Neural Information Pro-

- cessing Systems, 13 (2001), pp. 556–562.
- [27] C. LIN, *Projected gradient methods for nonnegative matrix factorization*, Neural computation, 19 (2007), pp. 2756–2779.
 - [28] J. LIU, J. LIU, P. WONKA, AND J. YE, *Sparse non-negative tensor factorization using column-wise coordinate descent*, Pattern Recognition, 45 (2012), pp. 649–656.
 - [29] J. NOCEDAL, *Updating quasi-Newton matrices with limited storage*, Mathematics of Computation, 35 (1980), pp. 773–782.
 - [30] J. NOCEDAL AND S. J. WRIGHT, *Numerical Optimization*, Springer, 2nd ed., 2006.
 - [31] P. PAATERO, *A weighted non-negative least squares algorithm for three-way “PARAFAC” factor analysis*, Chemometrics and Intelligent Laboratory Systems, 38 (1997), pp. 223–242.
 - [32] P. PAATERO AND U. TAPPER, *Positive matrix factorization: A non-negative factor model with optimal utilization of error estimates of data values*, Environmetrics, 5 (1994), pp. 111–126.
 - [33] M. SCHMIDT, D. KIM, AND S. SRA, *Projected Newton-type methods in machine learning*, in Optimization for Machine Learning, S. Sra, S. Nowozin, and S. J. Wright, eds., MIT Press, 2011, pp. 305–330.
 - [34] J. SUN, D. TAO, AND C. FALOUTSOS, *Beyond streams and graphs: Dynamic tensor analysis*, in KDD ’06, Proceedings of the 12th ACM SIGKDD International Conference on Knowledge Discovery and Data Mining, ACM, 2006, pp. 374–383.
 - [35] S. VAVASIS, *On the complexity of nonnegative matrix factorization*, SIAM Journal on Optimization, 20 (2009), pp. 1364–1377.
 - [36] M. WELLING AND M. WEBER, *Positive tensor factorization*, Pattern Recognition Letters, 22 (2001), pp. 1255–1261.
 - [37] Y. XU AND W. YIN, *A block coordinate descent method for multi-convex optimization with applications to nonnegative tensor factorization and completion*, Tech. Report 12-15, CAAM Rice University, Houston, TX, 2012.
 - [38] S. ZAFEIRIOU, *Algorithms for nonnegative tensor factorization*, in Tensors in Image Processing and Computer Vision, S. Aja-Fernandez, R. D. L. Garcia, D. Tao, and X. Li, eds., Springer, 2009, pp. 105–124.
 - [39] S. ZAFEIRIOU AND M. PETROU, *Nonnegative tensor factorization as an alternative Csiszar-Tusnady procedure: algorithms, convergence, probabilistic interpretations and novel probabilistic tensor latent variable analysis algorithms*, Data Mining and Knowledge Discovery, 22 (2011), pp. 419–460.
 - [40] R. ZDUNEK AND A. CICHOCKI, *Non-negative matrix factorization with quasi-Newton optimization*, in Eighth International Conference on Artificial Intelligence and Soft Computing, ICAISC, Springer, 2006, pp. 870–879.
 - [41] ———, *Nonnegative matrix factorization with constrained second-order optimization*, Signal Processing, 87 (2007), pp. 1904–1916.

Appendix A. Generating Synthetic Test Data.

The goal is to create artificial nonnegative factor matrices and from these compute a data tensor whose elements follow a Poisson distribution with multilinear parameters. Factorizing the data tensor should yield quantities that are close to the original factor matrices. The procedure is based on the work of [10].

The data tensor should be sparse, reflecting Poisson distributions whose probability of zero is not negligible. Each entry is a count of the number of samples assigned to this cell, out of a given total number of samples S . We generate factor matrices in each tensor mode and treat them as stochastic quantities to draw the S samples that provide data tensor counts.

Our generation procedure utilizes the function `create_problem` from Tensor Toolbox for Matlab [5], supplying a custom function for the `Factor_Generator` parameter (available as Matlab code from the authors). We create a multilinear model, $\mathcal{M} = [\boldsymbol{\lambda}; \mathbf{A}^{(1)} \dots \mathbf{A}^{(N)}]$, where $\mathbf{A}^{(n)} \in \mathcal{R}^{I_n \times R}$ and $\boldsymbol{\lambda} \in \mathcal{R}^R$, and sizes I_n and R are given. The model is generated by the following procedure:

Step 1 defines a strong preference for certain values of each index. As R increases, the relative probability of these indices is also increased so that they continue to stand out as strong preferences.

Step 10 rescales $\boldsymbol{\lambda}$ so that the ℓ_1 norms of the generated data tensor \mathcal{X} and

Algorithm 5 Generation of Synthetic Sparse Poisson Tensor Data

Given tensor sizes I_1, \dots, I_N , number of components R , and number of samples S .
Return a model $\mathcal{M} = [\boldsymbol{\lambda}; \mathbf{A}^{(1)} \dots \mathbf{A}^{(N)}]$, and corresponding sparse data tensor \mathcal{X} .

- 1: In each column of $\mathbf{A}^{(n)}$, choose 20% of the elements at random and set their value to $1 + 10Rx$, where x is a random value from a uniform distribution on $[0, 1]$. Set the other elements equal to the small constant 0.1.
 - 2: Choose random values for elements in $\boldsymbol{\lambda}$ from a uniform distribution on $[0, 1]$.
 - 3: Rescale each column of $\mathbf{A}^{(n)}$ so entries sum to 1, absorbing the scale factor into the corresponding element of $\boldsymbol{\lambda}$.
 - 4: Rescale the vector $\boldsymbol{\lambda}$ so entries sum to 1.
 - 5: **for** $s = 1, \dots, S$ **do**
 - 6: Treating $\boldsymbol{\lambda}$ as a distribution, choose a component r at random.
 - 7: Treating the r -th column of $\mathbf{A}^{(1)}$ as a distribution, choose an index i_1 with probability proportional to $\mathbf{a}_r^{(1)}$. Do the same for indices i_2, \dots, i_N , resulting in the index \mathbf{i} chosen with probability
$$P(\mathbf{i}) = a_{i_1 r}^{(1)} a_{i_2 r}^{(2)} \dots a_{i_N r}^{(N)}$$
 - 8: Increment the \mathbf{i} -th entry of \mathcal{X} by one.
 - 9: **end for**
 - 10: Rescale $\boldsymbol{\lambda} \leftarrow S\boldsymbol{\lambda}$ so that $\|\boldsymbol{\lambda}\|_1 = S$. ▷ Recall step 4 sets $\|\boldsymbol{\lambda}\|_1 = 1$.
-

K-tensor are the same in any mode- n unfolding. For example:

$$\begin{aligned} \|\mathbf{X}_{(1)}\|_1 &= \left\| \mathbf{A}^{(1)} \boldsymbol{\Lambda} (\mathbf{A}^{(N)} \odot \dots \odot \mathbf{A}^{(2)})^T \right\|_1 \\ &= \sum_{i=1}^{I_1} \sum_{r=1}^R \lambda_r a_{ri}^{(1)} \\ &= \sum_{r=1}^R \lambda_r \end{aligned}$$

The second equality uses the fact that rows of the Khatri-Rao product sum to 1 when columns of $\mathbf{A}^{(n)}$ sum to 1 (see the comments after equation (2.2)).